

A framework for geometrically non-linear gradient extended crystal plasticity coupled to heat conduction and damage

Magnus Ekh^{1a} and Swantje Bargmann^{2,3*}

¹*Division of Material and Computational Mechanics, Department of Applied Mechanics, Chalmers University of Technology, Gothenburg, Sweden*

²*Institute of Continuum Mechanics and Material Mechanics, Hamburg University of Technology, Germany*

³*Institute of Materials Research, Helmholtz-Zentrum Geesthacht, Germany*

(Received September 1, 2015, Revised December 5, 2015, Accepted December 15, 2015)

Abstract. Gradient enhanced theories of crystal plasticity enjoy great research interest. The focus of this work is on thermodynamically consistent modeling of grain size dependent hardening effects. In this contribution, we develop a model framework for damage coupled to gradient enhanced crystal thermo-plasticity. The damage initiation is directly linked to the accumulated plastic slip. The theoretical setting is that of finite strains. Numerical results on single-crystalline metal showing the development of damage conclude the paper.

Keywords: crystal plasticity; heat conduction; damage; gradient extension; dislocations

1. Introduction

Modeling and simulation of material behavior have been an important part of engineering research during the last decades. One area of large research interest is the computational modeling of crystalline materials which properties and macroscopic behavior are determined by the underlying microstructure. The development of innovative engineering materials (such as light construction materials) as well as the enhancement of classical materials (e.g., metals) requires deep knowledge on this issue.

Experimental data for low cycle fatigue for austenitic stainless steel is documented by Heino and Karlsson (2001). It is shown how microcracks initiate and orient along the slip planes. The low cycle fatigue experiments on a polycrystalline nickel-base alloy of Dunne, Wilkinson and Allen (2007) underline the importance of studying damage in crystalline materials as crack nucleation and growth strongly depend on the material's microstructure. The conclusion from experimental studies is that strain localization induces damage and crack nucleation. A further discussion about this can be found in Roters *et al.* (2010). The observations of Horstemeyer, Ramaswamy and Negrete (2003) clearly show the temperature dependence on void nucleation in aluminium. Moreover, Hou and Yue (2009) show that a temperature gradient results in a strain

*Corresponding author, Professor, E-mail: swantje.bargmann@tu-harburg.de

^aE-mail: magnus.ekh@chalmers.se

gradient as well as a damage gradient by investigating creep behavior in a thin-walled cylindrical single crystal superalloy.

Crystal plasticity, with slip system directions defined for each grain, is the standard choice of a constitutive model if modeling crystalline microstructures. The fact that standard crystal plasticity only accounts for the effect of the history of crystallographic slip, i.e., of statistically stored dislocations (SSDs), on the hardening behavior and, thus, is not able to capture size-dependent effects of Hall-Petch type, has motivated a number of workers to propose extensions to standard phenomenological plasticity and crystal plasticity. Prominent among these is the Mindlin-continuum- or strain-gradient-based extension of phenomenological plasticity of Fleck and Hutchinson (1997), which has also been applied to crystal plasticity in order to obtain a size dependent response.

There exists a wealth of literature with respect to gradient extended crystal plasticity, see, e.g., (Acharya and Beaudoin 2003, Bargmann and Ekh 2011, Borg 2007, Cermelli and Gurtin 2001, Ekh *et al.* 2007, Evers and Geers 2004a, Fleck *et al.* 1994, Kuroda and Tvergaard 2008, Gurtin 2004, Levkovitch and Svendsen 2006, Ohno and Okumura 2007, Yefimov and Giessen 2005). Crystal plasticity coupled to heat conduction has been studied in Håkansson and Ristinmaa (2008) and in terms of a gradient extended theory coupled to the thermal problem in Bargmann and Ekh (2013), McBride and Reddy (2015). Ekh and Runesson (2004) present a model for anisotropic damage coupled to crystal viscoplasticity; finite elastoplasticity with damage is studied by Clayton and McDowell (2004). Peerlings and Geers (2012) as well as Dimitrijevic and Hackl (2011) introduce isotropic, small strain models based on gradient enhanced plasticity and isotropic damage. Aslan and Forest (2011) present a constitutive model for damaging in a viscoplastic single crystal in the framework of small strains. The work of Welschinger (2011) treats gradient-type solids with intrinsic length scales within a variational framework, studying damage, fracture and plasticity.

Increasing plastic deformations in the material leads to degradation and softening. The softening or damage behavior has motivated the introduction of the research field damage mechanics, see e.g., Lemaître (1992). However, softening in the material leads to pathological localization and the finite element method will predict zero dissipation when refining the mesh, see e.g., Bazant and Lin (1988). Gradient extended formulations were applied resulting in a finite size of the localization zone. How to combine gradient extensions to capture both size-dependent hardening and finite size of localization zone is discussed in Peerlings and Geers (2012). In fact how to deal with the combination of these size-effects for crystal plasticity models of a crystal is the main issue of the current paper. Dissipative mechanisms such as plasticity and damage induce temperature changes in the material. The framework for thermo-mechanical coupling for gradient crystal plasticity described in Bargmann and Ekh (2013) is adopted. In the current contribution it is extended to also take into account the evolution of damage.

The paper is structured as follows: In Section 2 we introduce the underlying governing equations. We study the mechanical as well as the thermal problem and combine these with a damage model. The damage is proposed to be governed by the accumulated equivalent inelastic strain. Section 3 briefly sketches the finite element implementation. In particular, a dual mixed finite element method is applied. Finally, in Section 4 we illustrate the range of behaviors predicted by the proposed model by means of representative numerical examples.

2. Mathematical model

The governing equations of the model are set up in a thermodynamic framework. A detailed derivation for gradient extended crystal plasticity coupled to heat conduction is presented in Bargmann and Ekh (2013). The derivation with extension to damage is done in a straight forward fashion. In the following, only the main results are revisited and the enhancement to damage is discussed in order to avoid unnecessary repetitions.

2.1 Kinematics

We study the material behavior of a body B_0 that in general can consist of several grains. Its deformation is governed by the deformation gradient $\mathbf{F} := \nabla_0 \varphi(\mathbf{X}, t)$, where \mathbf{X} is a particle's position in the undeformed configuration B_0 and x denotes its spatial counterpart in the deformed (spatial) configuration B_t at time t . The deformation gradient is assumed to be multiplicatively split into an elastic \mathbf{F}^e (reversible) and a plastic (irreversible) part \mathbf{F}^p

$$\mathbf{F} = \mathbf{F}^e \cdot \mathbf{F}^p \quad (1)$$

see, e.g., Kröner (1960). The Jacobian of the deformation gradient is denoted $J = \det \mathbf{F}$. Relevant deformation measures are the right Cauchy-Green tensors

$$\mathbf{C} := \mathbf{F}^t \cdot \mathbf{F} \quad \text{and} \quad \mathbf{C}^e := [\mathbf{F}^e]^t \cdot \mathbf{F}^e \quad (2)$$

Moreover, we make use of the rate of deformation tensor \mathbf{d} which is defined as the symmetric part of the velocity gradient $\mathbf{l} := \dot{\mathbf{F}} \cdot \mathbf{F}^{-1}$, i.e.

$$\mathbf{d} := \mathbf{l}^{\text{sym}} = \frac{1}{2} \cdot [\mathbf{l} + \mathbf{l}^t] \quad (3)$$

From Eq. (1), the rate of deformation tensor \mathbf{d} is additively decomposed as $\mathbf{d} = \mathbf{d}^e + \mathbf{d}^p$ with $\mathbf{d}^e = [\dot{\mathbf{F}}^e \cdot [\mathbf{F}^e]^{-1}]^{\text{sym}}$ and $\mathbf{d}^p = [\mathbf{F}^e \cdot \dot{\mathbf{F}}^p \cdot [\mathbf{F}^p]^{-1} \cdot [\mathbf{F}^e]^{-1}]^{\text{sym}}$. A result that we need later is the time derivative of the elastic Cauchy-Green deformation \mathbf{C}^e which can be written as

$$\dot{\mathbf{C}}^e = 2[\mathbf{F}^e]^t \cdot \mathbf{d}^e \cdot \mathbf{F}^e \quad (4)$$

On the crystal level, $\underline{\gamma} := \{\gamma_1, \dots, \gamma_{n_{\text{slip}}}\}$ represent the plastic slips. The slip-system geometry is described by two unit vectors, i.e., the slip direction \mathbf{s}_α and slip-plane normal \mathbf{n}_α in the current configuration. On the intermediate configuration, $\bar{\mathbf{s}}_\alpha$ and $\bar{\mathbf{n}}_\alpha$ are defined from the push-forward operations

$$\bar{\mathbf{s}}_\alpha = \mathbf{F}_e \cdot \mathbf{s}_\alpha, \quad \bar{\mathbf{n}}_\alpha = [\mathbf{F}_e]^t \cdot \mathbf{n}_\alpha \quad (5)$$

We adopt the isoclinic assumption that slip directions on the intermediate and the reference configuration coincide.

2.2 Free energy function

Isotropic damage $d \in [0,1]$ is included in the model by adopting the concept of strain equivalence, see, e.g., Lemaître (1992). The damage is chosen to only affect the elastic part of the free energy, see, e.g., Lämmer and Tsakmakis (2000) for a discussion about alternatives. We introduce a free energy function which is additively decomposed into an elastic, a local inelastic, a non-local inelastic and a temperature contribution

$$\rho_0 \hat{\psi} := \rho_0 \hat{\psi}_e + \rho_0 \hat{\psi}_l + \rho_0 \hat{\psi}_{nl} + \rho_0 \hat{\psi}_{temp} \quad (6)$$

With

$$\begin{aligned} \rho_0 \hat{\psi}_e &= [1-d] \left[\frac{\mu}{2} [\mathbf{C}^e - \mathbf{I}] : \mathbf{I} \right] + \frac{\lambda}{2} \ln^2 J - \mu \ln J \\ \rho_0 \hat{\psi}_l &= \frac{1}{2} \sum_{\alpha, \beta} H_{\alpha\beta}^l \gamma_\alpha \gamma_\beta \\ \rho_0 \hat{\psi}_{nl} &= \frac{1}{2} \sum_{\alpha, \beta} l_\alpha l_\beta \nabla_0 \gamma_\alpha \mathbf{H}_{\alpha\beta}^g \nabla_0 \gamma_\beta \end{aligned} \quad (7)$$

$$\rho_0 \hat{\psi}_{temp} = \rho_0 c_0 \left[\theta - \theta_0 - \theta \ln \frac{\theta}{\theta_0} \right] - 3\alpha [\lambda + 2/3\mu] [\theta - \theta_0] \frac{\ln J}{J}$$

The elastic terms in $\rho_0 \hat{\psi}_e$ represent the classical free energy function of Neo-Hookean type characterized by the two Lamé constants λ and μ . The local contribution $\rho_0 \hat{\psi}_l$ is governed by the symmetric hardening modulus $H_{\alpha\beta}^l$ (which includes both self and latent hardening). The non-local term $\rho_0 \hat{\psi}_{nl}$ accounts for gradient latent-hardening effects via the symmetric $\mathbf{H}_{\alpha\beta}^g$ gradient hardening modulus

$$\mathbf{H}_{\alpha\beta}^g = [1-r] H_{\alpha\beta}^g \bar{\mathbf{s}}_\alpha \otimes \bar{\mathbf{s}}_\beta + r H_{\alpha\beta}^g \mathbf{I}. \quad (8)$$

The gradient hardening modulus contains an anisotropic and isotropic contribution. The latter gives a lower limit of the width of the localization zone orthogonal to the slip directions. This means that for a vanishing isotropic contribution (i.e., if the degree of isotropy in gradient hardening $r=0$), the width orthogonal to \mathbf{s}_α of the shear localization zone depends on the finite element mesh. Note that $H_{\alpha\beta}^l \neq H_{\alpha\beta}^g$, i.e., the gradient hardening matrix is not related to the usual interaction matrix for the classical hardening. $H_{\alpha\beta}^g$ are coefficients where the diagonal terms ($\alpha = \beta$) are related to the gradient self-hardening of the slip system α , whereas the off-diagonal elements ($\alpha \neq \beta$) induce gradient latent hardening between the slip systems α and β . For now and the remaining of the paper, we assume that all material parameters are temperature independent¹. l_α and l_β denote the internal length scales.

The first term in the $\hat{\psi}_{temp}$ accounts for the purely thermal behavior in terms of the specific heat

capacity c_0 . The last term introduces a thermo-mechanical coupling in terms of the thermal expansion coefficient α weighting the product of the bulk modulus $[\lambda + 2/3\mu]$ and the difference between the current temperature θ and the reference temperature θ_0 .

2.3 Stress measures

The second Piola-Kirchhoff stress on the intermediate configuration \mathbf{S}^e is obtained (via thermo-dynamical arguments) from

$$\mathbf{S}^e = 2 \frac{\partial \rho_0 \Psi}{\partial \mathbf{C}^e}. \quad (9)$$

The first Piola-Kirchhoff \mathbf{P} and Kirchhoff stress $\boldsymbol{\tau}$ are obtained from the current configuration via

$$\mathbf{P} = \mathbf{F}^e \cdot \mathbf{S}^e \cdot [\mathbf{F}^p]^{-t} \text{ and } \boldsymbol{\tau} = \mathbf{F}^e \cdot \mathbf{S}^e \cdot [\mathbf{F}^e]^t. \quad (10)$$

Further, we introduce the Schmid stress τ_α which is defined as the projection of the Kirchhoff stress $\boldsymbol{\tau}$ on the crystal system

$$\tau_\alpha = \mathbf{s}_\alpha \cdot \boldsymbol{\tau} \cdot \mathbf{n}_\alpha \quad (11)$$

and the effective Schmid stress (following the effective stress concept of Lemaître 1992)

$$\tilde{\tau}_\alpha = \frac{\tau_\alpha}{1-d}. \quad (12)$$

Last but not least, on thermodynamical arguments (see Ekh *et al.* 2007), we define the microstresses $\underline{\kappa} = \{\kappa_1, \dots, \kappa_{n_{slip}}\}$ and $\underline{\kappa}_\Gamma = \{\kappa_{\Gamma,1}, \dots, \kappa_{\Gamma,n_{slip}}\}$ as follows

$$\kappa_\alpha = \frac{\rho_0 \partial \Psi}{\partial \gamma_\alpha} - \text{Div} \left(\frac{\rho_0 \partial \Psi}{\partial \nabla_0 \gamma_\alpha} \right) \text{ in } B_{0,grain}, \quad \kappa_{\Gamma,\alpha} = \mathbf{N} \cdot \frac{\rho_0 \partial \Psi}{\partial \nabla_0 \gamma_\alpha} \text{ on the grain boundary } \Gamma_{0,grain} \quad (13)$$

where $\alpha = 1, 2, \dots, n_{slip}$ and \mathbf{N} is the outward normal to the grain boundary $\Gamma_{0,grain}$. The obtained relations for the stress measures given by the specific choice of free energy in Eq. (6) are stated in the Appendix, see Eq. (25).

2.4 Governing equation

The mechanical problem is governed by the equilibrium equations (assuming quasistatic conditions)

$$\text{Div} \mathbf{P} + \rho_0 \mathbf{b} = 0 \quad (14)$$

with \mathbf{b} being the volume force. In order to derive the heat equation, we start with the well-established fact that the balance of energy can be written as

$$\rho_0 \dot{\varepsilon} = -\text{Div} \mathbf{Q} + \mathbf{P} : \dot{\mathbf{F}} + \rho_0 r_{sh} \quad (15)$$

where ε is the mass specific internal energy density, r_{sh} is the external heat supply per unit mass and \mathbf{Q} is the material heat flux vector. The material heat flux vector is assumed to be determined by the temperature gradient $\nabla_0 \theta$ according to the isotropic Fourier's law $\mathbf{Q} := -k \nabla_0 \theta$ where k is the thermal conductivity. Inserting the definition of the Helmholtz free energy $\psi(\mathbf{C}_e, d, \gamma, \nabla_0 \gamma, \theta) := \varepsilon - \eta \theta$ and the thermodynamic relation² $\eta = -\frac{\partial \psi}{\partial \theta}$ into the balance of internal energy (15) leads to

$$\rho_0 c \dot{\theta} = -\text{Div} \mathbf{Q} + \rho_0 r_{sh} + \tau : \mathbf{d}^p - \underline{\kappa}^t \dot{\underline{\gamma}} + A \dot{d} + \rho_0 \theta \frac{\partial^2 \psi}{\partial \theta \partial \mathbf{C}^e} : \dot{\mathbf{C}}^e - \rho_0 \theta \frac{\partial \underline{\kappa}^t}{\partial \theta} \dot{\underline{\gamma}} + \rho_0 \theta \frac{\partial^2 \psi}{\partial \theta \partial d} \dot{d} \quad (16)$$

where we define the damage energy-conjugated variable A as $A = -\frac{\partial \rho_0 \psi}{\partial d}$. See Bargmann and Ekh (2013) for a detailed derivation in the context of gradient extended crystal thermoplasticity. As a consequence, damage leads to an additional increase in temperature because $A > 0$. The term involving the thermal gradient of the stress power $\frac{\partial^2 \psi}{\partial^2 \mathbf{C}^e} : \dot{\mathbf{C}}^e$ gives rise to the well known Gough-Joule effect (that is structural thermoelastic heating) which couples temperature evolution and elastic deformation.

2.5 Evolution equation

The relation for the damage variable d is proposed as

$$d = S \left[1 - \exp(-[\gamma_{eff} / \gamma_0]^m) \right] \quad (17)$$

Thus, the damage evolution is directly coupled to the effective plastic slip $\gamma_{eff} := \sqrt{\sum_{\alpha} \gamma_{\alpha}^2}$. S denotes the damage coefficient, γ_0 is the damage strain and m is the damage exponent. Due to relation (17), the damage variable d is approaching 1 asymptotically from below³ when increasing γ_{eff} . We adopt the standard crystal plasticity yield function on each slip system α as

$$\phi_{\alpha} := \tilde{\tau}_{\alpha} - \kappa_{\alpha} - Y_{\alpha} \quad (18)$$

which motivates the following relation for the (visco-)plastic slip rate of Norton type

$$\dot{\gamma}_{\alpha} = \frac{1}{t_*} \left\langle \frac{\phi_{\alpha}}{C_0} \right\rangle^n = \frac{1}{t_*} \left\langle \frac{\tilde{\tau}_{\alpha} - \kappa_{\alpha} - Y_{\alpha}}{C_0} \right\rangle^n \quad (19)$$

with $\gamma_{\alpha}(0) = 0$ (i.e., no initial slip) and t_* being the relaxation time, n the Norton exponent and C_0 denoting the drag stress. The current slip resistance on each slip system is $Y_{\alpha} + \kappa_{\alpha}$, where Y_{α} is the initial yield stress. The accumulated plastic slip is coupled to damage via Eq. (17) as local stresses may increase due to accumulation of dislocations and cause damage (see, e.g., Parisot *et*

al. 2004). Following Rice (1971), the evolution equation for the plastic part of the velocity gradient is chosen to be of associative type

$$\mathbf{L}_p = \sum_{\alpha=1}^{n_{slip}} \dot{\gamma}_\alpha \frac{\partial \phi_\alpha}{\partial \tau} = \sum_{\alpha=1}^{n_{slip}} \frac{\dot{\gamma}_\alpha}{1-d} [\mathbf{s}_\alpha \otimes \mathbf{n}_\alpha]. \quad (20)$$

Further, we introduce the slip gradients

$$\mathbf{g}_\alpha = \nabla_0 \gamma_\alpha. \quad (21)$$

The slip gradients \mathbf{g}_α are used as nodal degrees of freedom in the chosen finite element algorithm which is of dual mixed type. The slip gradient \mathbf{g}_α can be interpreted as edge dislocation densities.

3. Finite element implementation

In this Section, we shortly describe the chosen discretization method for the initial boundary value problem arising from the mathematical model. The solution method is based on finite elements for the spatial problem and finite differences for the temporal problem. For those readers who are interested in a detailed description, we refer to Bargmann *et al.* (2010), Ekh *et al.* (2007) where we explain the procedure in detail. In the following, only the basic steps are reiterated.

We apply a dual mixed finite element method: the geometrically necessary dislocation density g_α is modeled as a primary variable and the slip-system slip as a dependent constitutive quantity. Such a procedure is applied by, e.g., Bayley, Brekelmanns and Geers (2006), Ekh, Lillbacka and Runesson (2004), Evers, Brekelmanns and Geers (2004), Kuroda and Tvergaard (2006, 2008a), Vrech and Etse (2007) and Yefimov, Groma and Giessen (2004). A fully implicit backward Euler scheme is used for the temporal discretization.

A two-level Newton-Raphson iteration scheme is applied to the spatial discretization. Global FE-solutions of the equilibrium Eq. (14), the field equation for the geometrically necessary dislocation (21) and the heat Eq. (16) yield the displacement field $\mathbf{u}(\mathbf{X})$, the gradient $\mathbf{g}_\alpha(\mathbf{X})$ and the temperature $\theta(\mathbf{X})$ in the global nodes at time $t = t_n$. In a first loop, updated values of displacements \mathbf{u} , gradients \mathbf{g}_α and the temperature θ within each grain are computed. The fully discretized equations are coupled and the system is solved monolithically.

On the element level, an inner iteration loop is carried out. The purpose of this “local iteration loop” is to find updated values for the slip rates $\dot{\gamma}_\alpha$, the damage d as well as the stresses in each Gauss point, for given values of \mathbf{u} , \mathbf{g}_α and θ .

- 1.: Assume given values for the nodal displacement vector \mathbf{u}^n , the nodal vector of the gradients \mathbf{g}_α^n , the temperature θ^n and (converged) values $\dot{\gamma}_\alpha^n$ at time t_n
- 2.: Solve the governing equations for the nodal displacement vector \mathbf{u}^{n+1} , the gradients \mathbf{g}_α^{n+1} and the temperature θ^{n+1} in each grain via monolithic Newton–Raphson iterations.
 - “Local iteration loop”: For given $\mathbf{F}(\mathbf{u}^{n+1})$, \mathbf{g}^{n+1} , solve the flow rule (Eq. (19)) for $\dot{\gamma}^{n+1}$ and equation (Eq. (17)) for d^{n+1} in each element via monolithic Newton-Raphson iterations.
- 3.: If convergence, then set $n = n + 1$ and go to 1.

The flow rule is highly nonlinear and, thus, many iterations are needed. The application of a dual mixed finite element method allows to solve for the flow rule in the Gauß points on the element level which is more computationally efficient than to solve it in the nodes. If the flow rule instead would have been solved in the nodes, the deformation gradient and the stresses (which are computed in the Gauß points) would have to be averaged in order to obtain their values in the nodes.

4. Numerical examples

Finally, we turn to the elaboration of the proposed model by means of some selected representative examples. A single crystal with side length $L=10\ \mu\text{m}$ and two active slip systems (45° , 105°) is investigated. Both the local and the gradient hardening are assumed to be purely self-hardening, i.e., $H_{\alpha\beta}^l = H_\alpha^l \delta_{\alpha\beta}$ and $H_{\alpha\beta}^g = H_\alpha^g \delta_{\alpha\beta}$ as well as $l_\alpha = l \ \forall \alpha$. The gradient hardening is default a combination of slip hardening and isotropic hardening with $r=0.5$ but this value will be varied in the numerical examples in Subsection 4.5. The adopted material parameters are listed in Table 1. Plane strain is assumed. In order to trigger a non-homogeneous result the initial yield stress is slightly lower in the middle of the specimen. A simple tension test is performed with a maximum macroscopic strain $\gamma_{macro}=0.025$ with loading rate $\dot{\gamma}_{macro}=0.0125\ \text{s}^{-1}$. The temperature field is homogeneously initiated with $\theta_0=293\ \text{K}$ everywhere. The influence of boundary conditions, grain size, slip directions, the isotropy degree r and the coupled thermomechanical problem are investigated in Subsections 4.2-4.6.

Table 1 Material parameter values adopted for the gradient crystal plasticity model

Parameter	Symbol	Value	
Young's modulus	E	200	[GPa]
Poisson's ratio	ν	0.3	
Local hardening modulus	H_α^l	1000	[MPa]
Gradient hardening modulus	H_α^g	$4 \cdot 10^7$	[MPa]
Damage coefficient	S	1	
Internal length scale	l	10^{-2}	[μm]
Initial yield stress	Y_α	1000	[MPa]
Rate sensitivity parameter	n	1	
Damage exponent	m	2	
Damage strain	γ_0	$4 \cdot 10^{-2}$	
Drag stress	C_0	1	[MPa]
Relaxation time	t^*	10^3	[s]
Heat source	r_{sh}	0	[J/kg s]
Material density	ρ_0	7800	kg/m^3
Heat capacity	c	450	[J/kg K]
Thermal conductivity	k	60	[W/m K]
Thermal expansion coefficient	α	$1 \cdot 10^{-5}$	[K^{-1}]

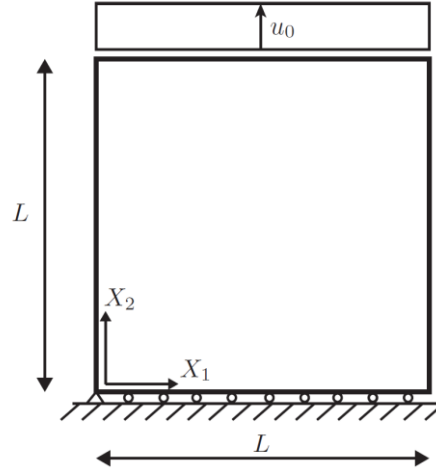


Fig. 1 The applied mechanical boundary conditions: The vertical boundaries $X_1=0, L$ are assumed to be traction free. At the upper boundary $X_2=L$, the displacement is controlled upwards and the traction is assumed to be free horizontally. On the lower boundary $X_2=0$, the lower left node is fixed horizontally and vertically. At the other nodes on the lower boundary, the displacement is fixed in vertical direction and the traction is assumed to vanish horizontally

4.1 Boundary conditions

Before proceeding to the results we define the geometry and the boundary conditions of the numerical example. The mechanical boundary conditions are illustrated in Fig. 1. The vertical displacement u_2 is zero on the lower boundary and controlled to u_0 on the upper boundary. The node in the lower left corner is fixed. The remaining boundary displacements are free.

The gradient hardening boundary conditions must be defined for the grain boundaries. In order to allow the damage to grow to the grain boundaries (inspired by the fact that low cycle fatigue often starts on free surfaces, see, e.g., Dunne and Allen (2007)) we mainly assume microfree conditions

$$\kappa_{\Gamma, \alpha} = 0 \text{ on } \Gamma_{0, \text{grain}} . \quad (22)$$

In other words, it is assumed that the microstress κ_{α} vanishes on these boundaries. For comparison, we also apply microhard conditions

$$\gamma_{\alpha} = 0 \text{ on } \Gamma_{0, \text{grain}} . \quad (23)$$

For more sophisticated gradient hardening boundary conditions, see e.g., Ekh, Bargmann and Grymer (2011). Furthermore, for the thermal problem we assume zero-flux on the grain's boundary $\Gamma_{0, \text{grain}}$ (used in Subsection 4.6)

$$\mathbf{Q} \cdot \mathbf{N} = 0 \text{ on } \Gamma_{0, \text{grain}} \quad (24)$$

which reflects on the average an adiabatic situation but with thermal conductivity inside the grain.

4.2 Influence of micro boundary conditions

First, we study the influence of the micro boundary condition on the plastic slip for a purely mechanical problem. The boundary conditions that we compare are microfree $\kappa_{\Gamma,\alpha}=0$ and microhard conditions $\gamma_\alpha=0$. The resulting stress-strain responses are shown in Fig. 2. The volume average of the first Piola-Kirchhoff stress component P_{11} is shown as a function of $\gamma_{macro} := u_0/L$. In the elastic region, both conditions predict the same material behavior. After yielding, microhard conditions map a stiffer response than microfree conditions until damage grows. With microhard conditions the material softens faster than with microfree conditions. The effective plastic slip γ_{eff} is depicted in Fig. 3. In both cases a slip band develops in the 45° slip direction. In case of microhard conditions, the slip vanishes at the all boundaries and accumulates in the center of the crystal. A second slip band in the 105° slip direction is clearly visible. The latter is absent in case of microfree conditions. Also, the slip distribution significantly differs as the slip accumulates in the lower left and upper right corners of the crystal. As damage is initiated by plastic slip, it evolves similar to the corresponding slip field, see Fig. 4. As clearly seen, the choice of the micro boundary condition is essential and should be chosen carefully depending the problem at hand.

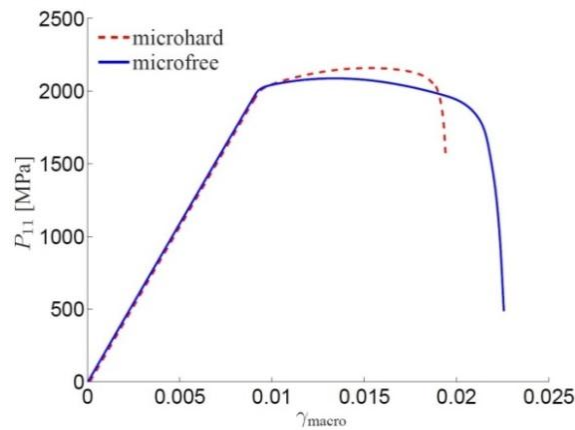


Fig. 2 Influence of microfree (solid line) and microhard (dashed line) boundary conditions on the homogenized stress-strain response. Crystal length $L=10 \mu\text{m}$. Slip directions 45° , 105° . Degree of isotropy $r = 0.5$

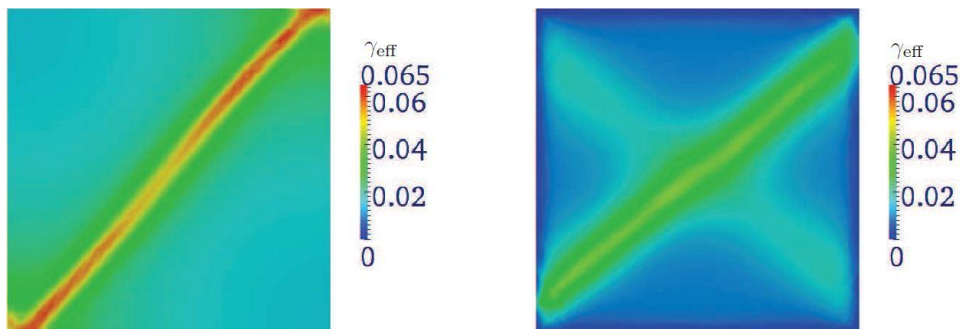


Fig. 3 Distribution of the accumulated plastic slip field for microfree (left) and microhard (right) boundary conditions. Crystal length $L=10 \mu\text{m}$. Slip directions 45° , 105° . Degree of isotropy $r = 0.5$

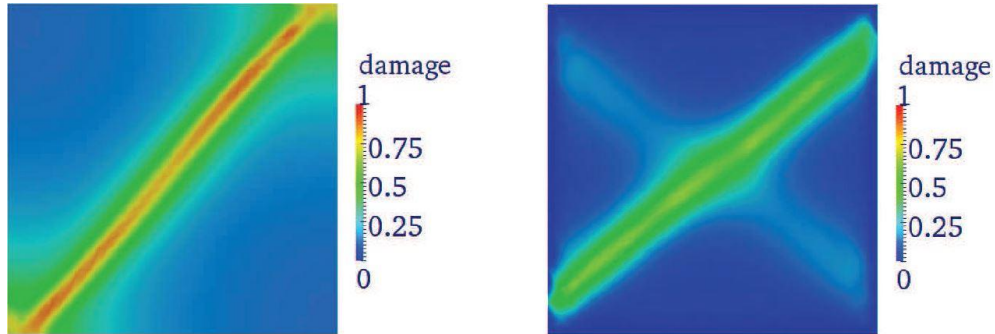


Fig. 4 Damage distribution for microfree (left) and microhard (right) boundary conditions. Crystal length $L=10\ \mu\text{m}$. Slip directions $45^\circ, 105^\circ$. Degree of isotropy $r=0.5$

4.3 Influence of grain size

Gradient extended crystal plasticity models have been developed in order to capture size effects. We have shown that our model predicts size-dependent hardening for the case of plasticity (Ekh *et al.* 2007, Bargmann and Ekh 2010, Bargmann and Ekh 2011, Husser and Bargmann 2014) as well as plasticity coupled to the thermal problem (Bargmann and Ekh 2013). Now, we investigate the influence of the grain size to plasticity coupled to damage. Microfree boundary conditions are assumed and the crystal's side length L is varied. As shown in Fig. 5, the larger the specimen is, the more pronounced is its softening behavior. Due to the microfree boundary conditions and a single crystal specimen, the size effect is only seen in the softening behavior. For microhard conditions, the size effect also appears in the hardening region. Moreover, the width of the slip band is close to constant whereby the relative width (with respect to L) increases with decreasing grain size, see Fig. 6. The corresponding damage distributions are depicted in Fig. 7.

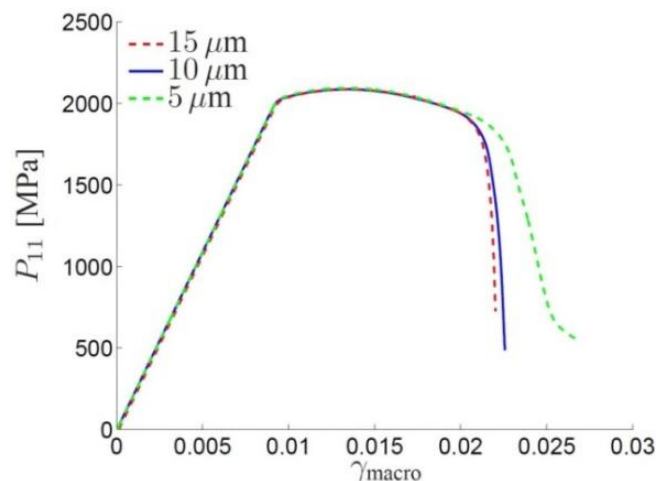


Fig. 5 Influence of grain size on the homogenized stress-strain response: exemplarily, it is shown for $L=5\ \mu\text{m}$, $L=10\ \mu\text{m}$, and $L=15\ \mu\text{m}$ (right). The larger the grain, the stronger the influence of damage resp. the softening. Microfree boundary conditions. Slip directions $45^\circ, 105^\circ$. $r=0.5$

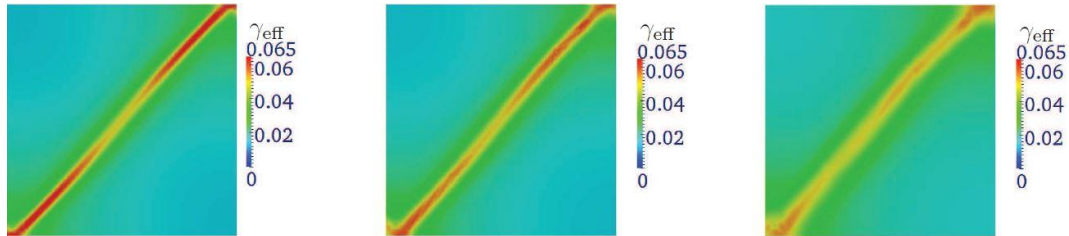


Fig. 6 Distribution of the accumulated plastic slip field for $L=15 \mu\text{m}$ (left), $L=10 \mu\text{m}$ (middle), and $L=5 \mu\text{m}$ (right). With decreasing grain size, the relative width of the slip band increases. Microfree boundary conditions. Slip directions 45° , 105° . $r=0.5$

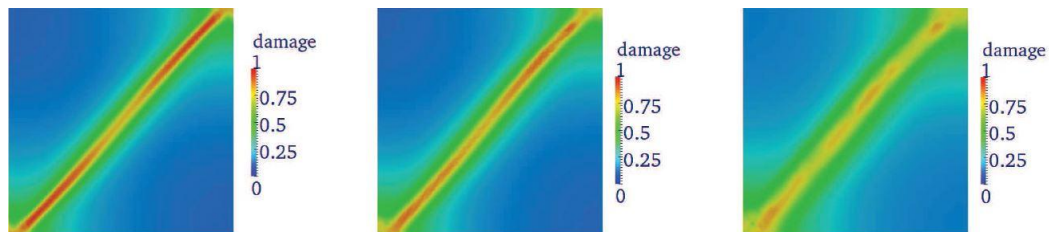


Fig. 7 Damage distribution for $L=15 \mu\text{m}$ (left), $L=10 \mu\text{m}$ (middle), and $L=5 \mu\text{m}$ (right). With decreasing grain size, the relative width of the slip band increases. Microfree boundary conditions. Slip directions 45° , 105° . $r=0.5$

4.4 Influence of slip orientation

We now keep the specimen's side length fixed at $L=10 \mu\text{m}$ and assume microfree boundary conditions. The slip directions are varied: 45° , 105° resp. 10° , 70° resp. -30° , 30° . The influence is clearly visible in the stress-strain response (Fig. 8) as well as the distribution of the accumulated plastic slip (Fig. 9) and damage (Fig. 10). Some grains are better orientated for (resp. against) damage generated by plasticity than others, as the damage evolution inside the grain depends on the slip directions. As one consequence, some grains behave much stiffer than others, see Fig. 8.

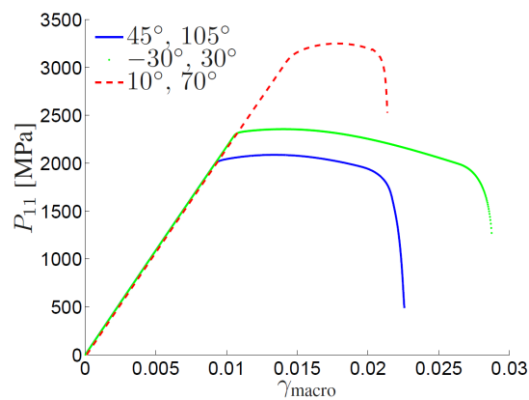


Fig. 8 A strong influence of slip directions on the homogenized stress-strain response is visible. Microfree boundary conditions. $L=10 \mu\text{m}$. $r=0.5$

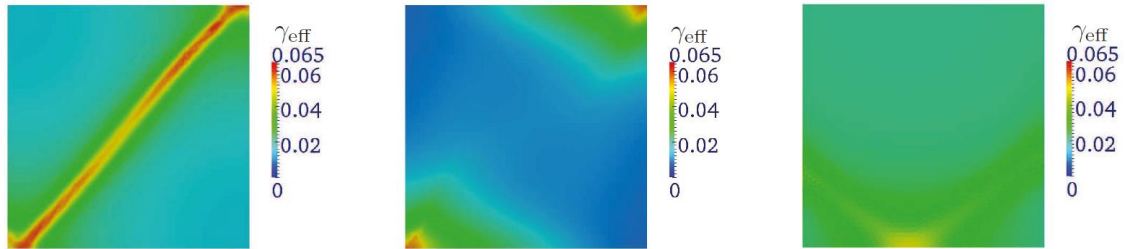


Fig. 9 Influence of slip directions on the distribution of the accumulated plastic slip field for 45°, 105° (left), 10°, 70° (middle) and -30°, 30° (right). Microfree boundary conditions. $L=10 \mu\text{m}$. $r=0.5$

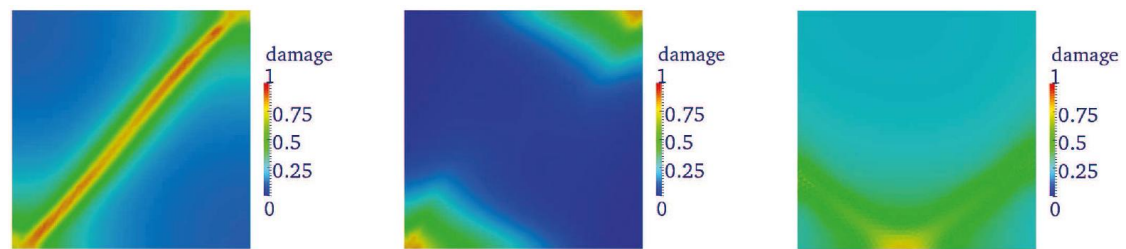


Fig. 10 Influence of slip directions on the damage distribution for 45°, 105° (left), 10°, 70° (middle) and -30°, 30° (right). Microfree boundary conditions. $L=10 \mu\text{m}$. $r=0.5$

4.5 Influence of slip resp. isotropic hardening

Here, we investigate the influence of anisotropic slip-direction based hardening versus isotropic hardening. This is controlled via the isotropy degree r . The results are shown in Figs. 11-13. The assumed slip directions are 45° and 105°, grain size $L=10 \mu\text{m}$ and microfree boundary conditions are assumed. For $r \neq 0$, the numerical results are mesh-independent. However, without the isotropic contribution (i.e., $r=0$), the results, in particular the width of the shear localization band, depend on the refinement of the finite element mesh.

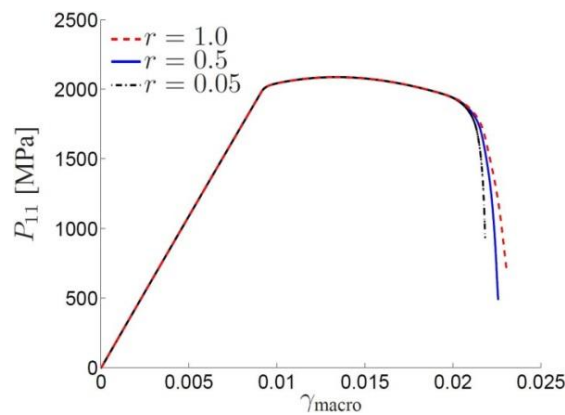


Fig. 11 Influence of isotropy degree r on the homogenized stress-strain response. Microfree boundary conditions. $L=10 \mu\text{m}$. Slip directions 45°, 105°

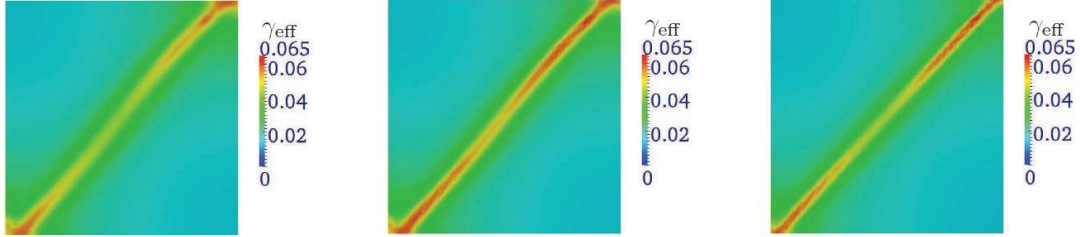


Fig. 12 Plastic slip field for $r=1$ (left), $r=0.5$ (middle) and $r=0.05$ (right). A larger isotropic contribution gives a broader width of the shear band. Microfree boundary conditions. $L=10\ \mu\text{m}$. Slip directions 45° , 105°

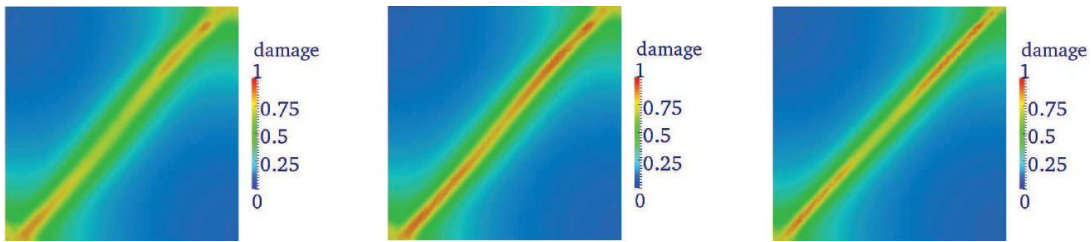


Fig. 13 Damage distribution for $r=1$ (left), $r=0.5$ (middle) and $r=0.05$ (right). A larger isotropic contribution gives a broader width of the shear band. Microfree boundary conditions. $L=10\ \mu\text{m}$. Slip directions 45° , 105°

4.6 The fully coupled problem: gradient crystal plasticity coupled to temperature and damage

The experiments of Bodelot *et al.* (2011) show an instantaneous coupling between strain gradients and thermal dissipation in a polycrystalline metal. Further, Horstemeyer, Ramaswamy and Negrete (2003) prove the influence of temperature on the damage behavior of polycrystals. Consequently, as a next step, we take the temperature development inside the specimen into account in the following. The influence of loading rate, grain size and boundary conditions on the temperature field have been studied in Bargmann and Ekh (2013). Therefore, this is not repeated for the gradient crystal plasticity coupled to temperature and damage as the results will be accordingly. Thus, in the following, we only give one example of the fully coupled problem for the sake of completeness. The set-up of the example for damage coupled to gradient extended crystal plasticity assumes slow loading. Thus, the heat equilibrates faster than the damage and the plastic slip develop.

We therefore change to a faster loading rate ($\dot{\gamma}_{macro} = 25 \cdot 10^4 \text{s}^{-1}$) and relaxation time ($t_* = 10\text{s}^{-4}$) for the example in this section. The stress-strain behavior is illustrated in Fig. 14. Heat is produced due to plastic yielding and it is strain rate dependent (Bargmann and Ekh 2013). We perform the simulations without accounting for thermal expansion as temperature change due to elastic effects is negligible once plastic flow is developed (McBride and Reddy 2015) and, by this, avoid further nonlinear coupling of the highly nonlinear and strongly coupled set of equations. The damage as well as the temperature evolution are driven and strongly influenced by the plastic strain, see Fig. 15. The relation between the plastic slip and the temperature is nontrivial. The more plastic slip arises, the more heat is generated, i.e., in the area of the slip band (which coincides with the most damaged area), the specimen heats up most.

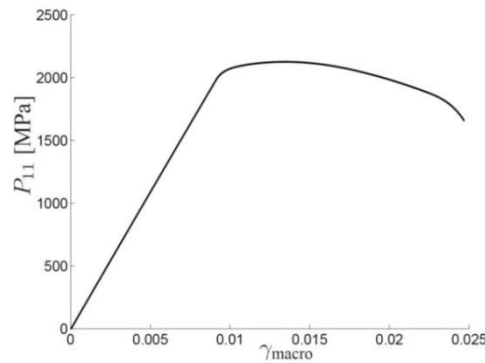


Fig. 14 Stress-strain response for the fully coupled problem of gradient crystal thermo-plasticity with damage. Microfree boundary conditions. $L=10\ \mu\text{m}$. Slip directions $45^\circ, 105^\circ$. $r=0.5$

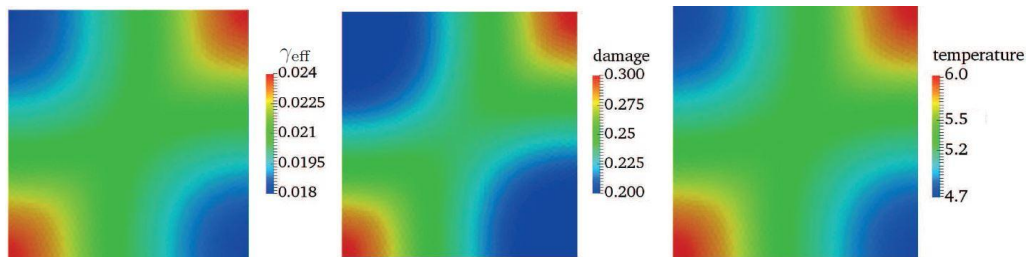


Fig. 15 Fully coupled problem: distribution of the accumulated plastic slip (left), damage (middle) and temperature increase (right). Microfree boundary conditions. $L=10\ \mu\text{m}$. Slip directions $45^\circ, 105^\circ$. $r=0.5$

5. Conclusions

As damage and temperature evolution play an important role in the material's overall behavior (see, e.g., the experimental observations of Horstemeyer, Ramaswamy and Negrete (2003)), the mechanical problem is coupled to heat conduction and damage. We present a multi-physics model for size-dependent hardening in crystals accounting for temperature distribution and damage evolution. The typical hardening behavior of the gradient extended crystal plasticity model is strongly affected by the evolving damage. The damage inside the material is driven by the plastic strain and leads to softening. Moreover, changes in the temperature field influence the deformation field as well as the damage and vice versa, i.e., the coupling is manifold. The damage development inside the grain depends on the slip directions, i.e., some grains are better orientated for damage generated by plasticity than others. The model can reasonably predict plastic slip, damage and temperature evolution for single crystals. The extension to polycrystals is straightforward.

Acknowledgements

Part of this research was done while SB visited Chalmers University of Technology (Gothenburg, Sweden), whose hospitality is gratefully acknowledged. SB gratefully acknowledges financial support from the German Research Foundation (DFG) via SFB 986 "M³", project B6. Furthermore, the simulations were performed on resources provided by the Swedish National

Infrastructure for Computing (SNIC) at Chalmers Centre for Computational Science and Engineering (C3SE).

References

- Acharya, A., Bassani, J.L. and Beaudoin, A. (2003), "Geometrically necessary dislocations, hardening, and a simple gradient theory of crystal plasticity", *Scripta Materialia*, **48**(2), 167-172.
- Aslan, O. and Forest, S. (2011), "The micromorphic versus phase field approach to gradient plasticity and damage with application to cracking in metal single crystals", *Multiscale Methods in Computational Mechanics*, Springer, Netherlands.
- Bargmann, S., Ekh, M., Runesson, K. and Svendsen, B. (2010), "Modeling of polycrystals with gradient crystal plasticity: A comparison of strategies", *Philosoph. Magaz.*, **90**(10), 1263-1288.
- Bargmann, S., Svendsen, B. and Ekh, M. (2011), "An extended crystal plasticity model for latent hardening in polycrystals", *Comput. Mech.*, **48**(6), 631-645.
- Bargmann, S. and Ekh, M. (2013), "Microscopic temperature field prediction during adiabatic loading in a gradient extended crystal plasticity theory", *Int. J. Solid. Struct.*, **50**(6), 899-906.
- Bayley, C., Brekelmans, W. and Geers, M. (2006), "A comparison of dislocation induced back stress formulations in strain gradient crystal plasticity", *Int. J. Solid. Struct.*, **43**(24), 7268-7286.
- Bazant, Z. and Lin, F.-B. (1988), "Non-local yield limit degradation", *Int. J. Numer. Meth. Eng.*, **26**(8), 1805-1823.
- Bodelot, L., Charkaluk, E., Sabatier, L. and Dufrenoy, P. (2011), "Experimental study of heterogeneities in strain and temperature fields at the microstructural level of polycrystalline metals through fully-coupled full-field measurements by digital image correlation and infrared thermography", *Mech. Mater.*, **43**(11), 654-670.
- Borg, U. (2007), "A strain gradient crystal plasticity analysis of grain size effects in polycrystals", *Eur. J. Mech. Solid.*, **26**(2), 313-324.
- Cermelli, P. and Gurtin, M.E. (2001), "On the characterization of the geometrically necessary dislocations in finite plasticity", *J. Mech. Phys. Solid.*, **49**(7), 1539-1568.
- Clayton, J. and McDowell, D. (2004), "Homogenized finite elastoplasticity and damage: theory and computations", *Mech. Mater.*, **36**(9), 799-824.
- Dimitrijevic, B.J. and Hackl, K. (2011), "A regularization framework for damage-plasticity models via gradient enhancement of the free energy", *Int. J. Numer. Meter. Biol. Eng.*, **27**(8), 1199-1210.
- Dunne, F.P.E., Wilkinson, A.J. and Allen, R. (2007), "Experimental and computational studies of low cycle fatigue crack nucleation in a polycrystal", *Int. J. Plast.*, **23**(2), 273-295.
- Ekh, M., Lillbacka, R. and Runesson, K. (2004), "A model framework for anisotropic damage coupled to crystal (visco)plasticity", *Int. J. Plast.*, **20**(12), 2143-2159.
- Ekh, M., Grymer, M., Runesson, K. and Svedberg, T. (2007), "Gradient crystal plasticity as part of the computational modeling of polycrystals", *Int. J. Numer. Meter. Eng.*, **72**(2), 197-220.
- Ekh, M., Bargmann, S. and Grymer, M. (2011), "Influence of grain boundary conditions on modeling of size-dependence in polycrystals", *Acta Mechanica*, **218**(1-2), 103-113.
- Evers, L.P., Brekelmanns, W.A.M. and Geers, M.G.D. (2004), "Non-local crystal plasticity model with intrinsic ssd and gnd effects", *J. Mech. Phys. Solid.*, **52**(10), 2379-2401.
- Evers, L.P., Brekelmanns, W.A.M. and Geers, M.G.D. (2004a), "Scale dependent crystal plasticity framework with dislocation density and grain boundary effects", *Int. J. Solid. Struct.*, **41**(18), 5209-5230.
- Fleck, N.A., Muller, G.M., Ashby, M.F. and Hutchinson, J.W. (1994), "Strain gradient plasticity: theory and experiment", *Acta Metallurgica et Materialia*, **42**(2), 475-487.
- Fleck, N.A. and Hutchinson, J.W. (1997), "Strain gradient plasticity", *Adv. Appl. Mech.*, **33**, 295-361.
- Gurtin, M.E. (2004), "A gradient theory of small-deformation isotropic plasticity that accounts for the Burgers vector and for dissipation due to plastic spin", *J. Mech. Phys. Solid.*, **52**(11), 2545-2568.

- Håkansson, P., Wallin, M. and Ristinmaa, M. (2008), "Prediction of stored energy in polycrystalline materials during cyclic loading", *Int. J. Solid. Struct.*, **45**(6), 1570-1586.
- Heino, S. and Karlsson, B. (2001), "Cyclic deformation and fatigue behavior of 7Mo-0.5N superaustenitic stainless steel characteristics and development of the dislocation structures", *Acta Materialia*, **49**(2), 353-363.
- Horstemeyer, M., Ramaswamy, S. and Negrete, M. (2003), "Using a micromechanical finite element parametric study to motivate a phenomenological macroscale model for void/crack nucleation in aluminum with a hard second phase", *Mech. Mater.*, **35**(7), 675-687.
- Hou, N., Wen, Z. and Yue, Z. (2009), "Creep behavior of single crystal superalloy specimen under temperature gradient condition", *Mater. Sci. Eng.*, **A510**, 42-45.
- Husser, E., Lilleodden, E. and Bargmann, S. (2014), "Computational modeling of intrinsically induced strain gradients during compression of c-axis oriented magnesium single crystal", *Acta Materialia*, **71**, 206-219.
- Kröner, E. (1960), "Allgemeine kontinuumstheorie der versetzungen und eigenspannungen", *Archiv. Ration. Mech. Anal.*, **4**(1), 273-334.
- Kuroda, M. and Tvergaard, V. (2006), "Studies of scale dependent crystal viscoplasticity models", *J. Mech. Phys. Solid.*, **54**(9), 1789-1810.
- Kuroda, M. and Tvergaard, V. (2008), "On the formulations of higher-order strain gradient crystal plasticity models", *J. Mech. Phys. Solid.*, **56**(4), 1591-1608.
- Kuroda, M. and Tvergaard, V. (2008a), "A finite deformation theory of higher-order gradient crystal plasticity", *J. Mech. Phys. Solid.*, **56**(8), 2573-2584.
- Lämmer, H. and Tsakmakis, C. (2000), "Discussion of coupled elastoplasticity and damage constitutive equations for small and finite deformations", *Int. J. Plast.*, **16**(5), 495-523.
- Lemaître, J. (1992), *A Course on Damage Mechanics*.
- Levkovitch, V. and Svendsen, B. (2006), "On the large-deformation- and continuum-based formulation of models for extended crystal plasticity", *Int. J. Solid. Struct.*, **43**(24), 7246-7267.
- McBride, A., Bargmann, S. and Reddy, D. (2015), "A computational investigation of a model of single-crystal gradient thermoplasticity that accounts for the stored energy of cold work and thermal annealing", *Compos. Mech.*, **55**(4), 755-769.
- Ohno, N. and Okumura, D. (2007), "Higher-order stress and grain size effects due to self-energy of geometrically necessary dislocations", *J. Mech. Phys. Solid.*, **55**(9), 1879-1898.
- Parisot, R., Forest, S., Pineau, A., Grillon, F., Demonet, X. and Mategne, J.-M. (2004), "Deformation and damage mechanisms of zinc coatings on hot-dip galvanized steel sheets: Part II. Damage modes", *Metal. Mater. Trans. A*, **35**(3), 813-823.
- Peerlings, R., Poh, L. and Geers, M. (2012), "An implicit gradient plasticity-damage theory for predicting size effects in hardening and softening", *Eng. Fract. Mech.*, **95**, 2-12.
- Rice, J. (1971), "Inelastic constitutive relations for solids: an internal-variable theory and its application to metal plasticity", *J. Mech. Phys. Solid.*, **19**(6), 433-455.
- Roters, F., Eisenlohr, P., Hantcherli, L., Tjahjanto, D., Bieler, T. and Raabe, D. (2010), "Overview of constitutive laws, kinematics, homogenization and multiscale methods in crystal plasticity finite-element modeling: Theory, experiments, applications", *Acta Materialia*, **58**(4), 1152-1211.
- Vrech, S.M. and Etse, G. (2007), "FE approach for thermodynamically consistent gradient-dependent plasticity", *Latt. Am. Appl. Res.*, **37**(2), 127-132.
- Welschinger, F. (2011), "A variational framework for gradient-extended dissipative continua. Application to damage mechanics, fracture, and plasticity", Ph.D. thesis, University of Stuttgart, Germany.
- Yefimov, S., Groma, I. and Giessen, E. van der (2004), "A comparison of a statistical-mechanics based plasticity model with discrete dislocation plasticity calculations", *J. Mech. Phys. Solid.*, **52**(2), 279-300.
- Yefimov, S. and Giessen, E. van der (2005), "Multiple slip in a strain-gradient plasticity model motivated by a statistical-mechanics description of dislocations", *Int. J. Solid. Struct.*, **42**(11), 3375-3394.

Appendix

The choice of Helmholtz' free energy in Eq. (6) results in following relations

$$\begin{aligned}
 \tau &= [1-d] \left[\mu [\mathbf{b}^e - \mathbf{I}] + \lambda \ln(J) \mathbf{I} \right] - 3\alpha \left[\lambda + \frac{2}{3} \mu \right] [\theta - \theta_0] \left[1 - \ln(J) \right] \frac{\mathbf{I}}{J}, \\
 \kappa_\alpha &= \sum_\beta H_{\alpha\beta}^l \gamma_\beta - r H_{\alpha\beta}^g l_\alpha l_\beta \bar{\mathbf{s}}_\beta \cdot \nabla_0 \mathbf{g}_\beta \cdot \bar{\mathbf{s}}_\alpha - [1-r] H_{\alpha\beta}^g l_\alpha l_\beta \text{Div}(\mathbf{g}_\beta), \\
 \kappa_{\Gamma,\alpha} &= \sum_\beta r H_{\alpha\beta}^g l_\alpha l_\beta [\mathbf{N} \cdot \bar{\mathbf{s}}_\alpha] \cdot [\mathbf{g}_\beta \cdot \bar{\mathbf{s}}_\beta] + [1-r] H_{\alpha\beta}^g l_\alpha l_\beta \mathbf{N} \cdot \mathbf{g}_\beta, \\
 A &= \frac{\mu}{2} [\mathbf{C}^e - \mathbf{I}] : \mathbf{I} + \frac{\lambda}{2} \ln^2 J - \mu \ln J
 \end{aligned} \tag{25}$$